Compton Scattering

Tony Hyun Kim
MIT Department of Physics
(Dated: December 1, 2008)

We perform scattering of 661.6keV photons from electrons. The Compton wavelength shift is observed in the scattered beam, which rules out the classical EM scattering model. Based on the fit to the shift formula, we estimate the electron rest mass to be $E_e = (514.3 \pm 8.3)$ keV/c^2. We also consider the angular dependence of the scattering cross-section, in which the Klein-Nishina formula prevails over the classical dipole radiation model at $\chi^2_\nu = 1.8$ vs. $\chi^2_\nu = 61.0$.

1. INTRODUCTION

By the beginning of the twentieth century, light was firmly established as a wave phenomenon governed by the Maxwell's equations. Qualitative features of light-matter interaction was successfully explained by the *Rayleigh scattering* model, in which matter is considered to be an electric dipole driven by the incident EM radiation. Classical analyses of this type yielded specific predictions for the scattering cross-section, i.e. the dipole radiation pattern for light scattering from matter. Additionally, a basic result of the classical analysis is that no wavelength shifts can occur since the governing physics is linear (i.e. the Maxwell's equations and the harmonic oscillator model of an electric dipole).

In this investigation, we perform *Compton scattering* of γ-rays from electrons, which in 1920 dramatically demonstrated the deficiencies of the wave model. In contrast to the classical predictions, we observe variation in the scattered photon wavelength in accordance with the Compton shift formula (Eq. 1). We have also tested the angular dependence of the scattering rate to the Klein-Nishina cross-section as well as the classical prediction. We observe a decisive preference for the Klein-Nishina formula (at $\chi^2_\nu = 1.8$ vs. $\chi^2_\nu = 61.04$).

2. THEORETICAL BACKGROUND

Following Compton, we apply the basic results of quantum mechanics and relativity to the scattering process, rather than the classical equations. In the modern picture, light is composed of particle-like photons, containing energy $E = hc/\lambda$ as predicted by QM. Light also possesses momentum according to the relativistic equation $p = E/c = h/\lambda$, valid for particles of zero rest mass.

2.1. Wavelength shift

In the Compton analysis, the scattering process is analyzed as a collision of two particles: an incident photon and an electron initially at rest. As usual, we invoke the conservation of energy and momentum in the collision process. While the analysis is trivial, Compton's insight was then to incorporate the momentum-wavelength equa-

tion, yielding the wavelength shift formula for the scattered photon:

$$\Delta\lambda = \frac{h}{m_e c}\left(1 - \cos\theta\right) \tag{1}$$

where m_e is the mass of the electron, and θ is the angle between the incident and scattered trajectories. Remarkably, this simple analysis predicts a nonlinear response (i.e. a frequency shift) in the scattering process. This unequivocally shows that the underlying physics goes beyond the linear physics of Maxwell's equations. Finally, for later use, it will be useful to re-express Eq. 1 for the final photon energy, as in:

$$E_f = \frac{1}{E_i^{-1} + E_e^{-1}\left(1 - \cos\theta\right)} \tag{2}$$

where E_i is the incident photon energy, and $E_e = m_e c^2$ is the rest energy of the electron.

2.2. Scattering cross-section

In the classical Rayleigh model, the scattering is due to a driven dipole oscillator. Recall that the radiation pattern of dipole radiation contains a $\sin^2\theta$ dependence, where θ is the angle from the dipole axis. Since this axis will be perpendicular to the incident photon direction, it follows that the photon scattering rates will be symmetric in the forward and backward directions.

The classical prediction can be contrasted against the Klein-Nishina cross-section, derived from relativistic QFT.[1] In this work, we show that the Klein-Nishina formula is experimentally preferred over the Rayleigh model. For the incident photon energy used in our experiment, the Klein-Nishina formula is strongly forward-peaked ($\theta \leq 90°$), and shows significant angular dependence in the forward direction. The cross-section becomes uniform for larger scattering angles. Based on this result, we will argue later that the optimal regime for testing the Compton shift (Eq. 2) are the large-angle deflections.

3. EXPERIMENTAL SETUP

The apparatus consisted of a ^{137}Cs source, emitting 661.6keV photons. As shown in Figure 1, the source was

aimed at the "target" PMT. The scattered photons from the target PMT were detected by the "scatter" PMT, which could be positioned at various angles.
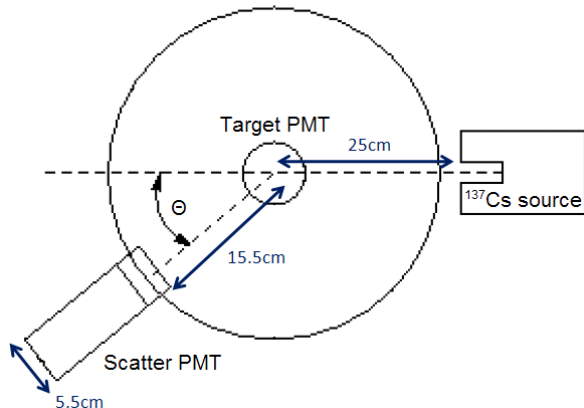

FIG. 1: Schematic of the experimental apparatus. The ^{137}Cs source is aimed at the "target" PMT, which scatters photons. Some of the scattered light is collected by the "scatter" PMT which is free to rotate about the apparatus. The dimensions given are those of the Compton A apparatus. Figure from [2]

Because the Compton event involves two particles, the scattered photon and the recoiling electron, we were able to use coincidence techniques in order to improve the signal-to-noise ratio. The scattered photon is detected in the scatter PMT, while the recoiling electron is detected in the target PMT. From the two ensuing signal chains, we generated a "coincidence" (AND) logic signal, which gated the PC-based MCA to be operational only when *both* PMTs had registered hits. One drawback of this setup is that, in order to produce the coincidence logic, we had to employ a discriminator in the signal chain. Since the kinetic energy of the recoil electron can be arbitrarily small (i.e. below the discriminator set-point) for smaller deflection angles, we should expect such runs to yield less reliable data.

The scattering experiments were performed at various angles for $10-15$ minutes. Suspecting shot-to-shot drifts in the calibration, we calibrated the MCA with ^{22}Na, ^{133}Ba and ^{137}Cs test sources with each run. We have found only minor drifts of the MCA channel calibration, of up to 2keV.

We have used both Compton apparatuses in Junior Lab (Compton A and B) in order to conduct the experiment. We first discuss some geometric considerations that are common to both setups. We have found that both ^{137}Cs sources produce divergent beams. The FWHM of both beam profiles was approximately 12°. The diameter of the PMTs used were 5.5cm. (See Fig. 1.) It is clear that the finite geometries in the experiment necessitates numerous convolutions for an accurate assessment of the scattering-rate results. The geometric factors are also important for the Compton shift experiment, since the forward-preference of the (Klein-

Nishina) cross-section can cause underestimation of the energy shifts. In our analysis of the low-angle Compton-shift data, we have observed such biases. In our work, we mainly report results from high-angle measurements so that the various complications of low-angle scattering can be bypassed.

Finally, we note that Compton B offers two distinct advantages over Compton A. First, the arm length of the scatter PMT (to the target PMT) is 25.2cm in Compton B, as opposed to 15.5cm of Compton A. Hence, Compton B offers higher angular specificity since the detector exposes a smaller solid angle to the scattering center. Secondly, we have characterized the intensities of the two ^{137}Cs sources, and found that the Compton B source was 2.4 times more intense than that of Compton A. This deficiency was fatal for Compton A: we were not able to collect a recognizable signal beyond $\theta \approx 70°$ on this apparatus.

4. RESULTS AND DISCUSSION

4.1. Spectrum fitting and MCA calibration

As in Figure 2, individual peaks in the MCA spectrum were generally characterized by a Gaussian function. However, we have found that the spectra includes additional complications. In the spectrum of the ^{133}Ba test source, for instance, the wings of the various lines interfered with one another as to produce a nonuniform baseline. We have numerically accomodated for such complications by using as the fitting model a superposition of a Gaussian on top of a linear "background" function.
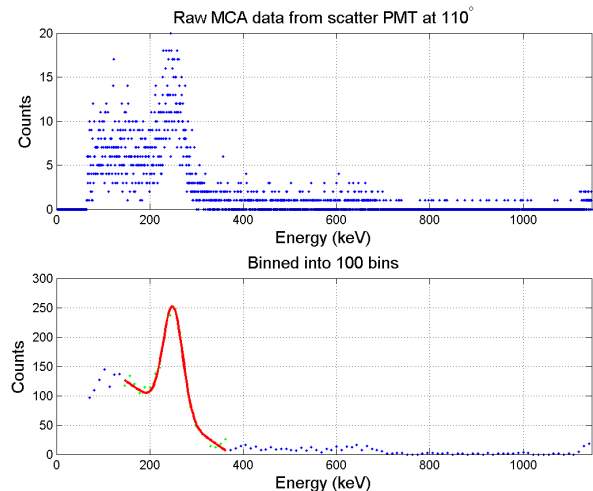

FIG. 2: The top panel shows the raw spectrum from the scatter PMT for the 110° run. Below, the raw spectrum was collected into 100 energy bins in order to make the photopeak more evident. The data was fitted against the superposition of Gaussian and linear functions. This particular fit produced $\chi^2_\nu = 2.25$, and mean energy $E = 249.0 \pm 1.1$keV.

4.2. Wavelength shift

Figure 3 shows the scattered photon energies as a function of deflection angle. Note that the variation in energy implies a shift in wavelength, hence we have already eliminated classical scattering as a viable model. The smaller-angle runs were performed with the Compton A apparatus, while the large angles were obtained using the Compton B apparatus. Fig. 3 also shows fits of the data to the Compton shift formula (Eq. 2) with E_i and E_e as fit parameters.
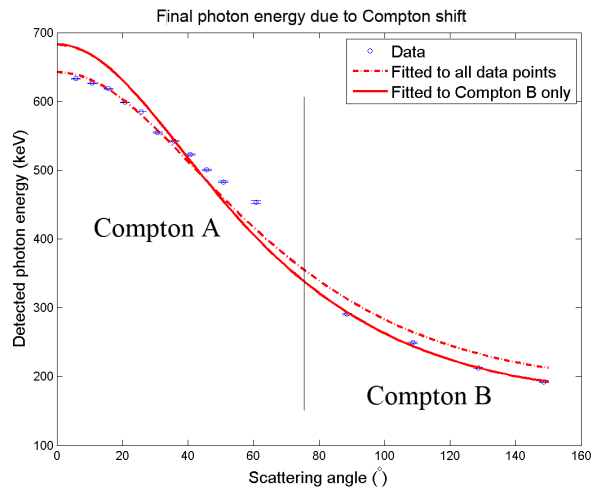

FIG. 3: Final scattered photon energy as a function of deflection angle. Our primary machine was Compton A, which yielded small-angle data. Compton B was used to investigate large-angle scattering. The measurements were fitted against $f(\theta) = \left[E_i^{-1} + E_e^{-1}(1 - \cos\theta)\right]^{-1}$ with E_i and E_e as fitting parameters. The dotted curve is the resulting fit for all data points. The solid curve is the fit to Compton B only.

The fit to both Compton A and B data displays the systematic effects we have already discussed at low angles. Firstly, it is clear that each measurement underestimates the Compton shift to some degree; this is to be expected since the underlying cross-section heavily favors lower-angle scattering. For any fixed scatter PMT position θ, the scattering process will actually involve some interval of angles in the neighborhood of θ. The forward-biased cross-section then selects some "effective mean" angle that is smaller than the actual experimental angle. Secondly, the fit estimates the incident photon energy to be $E_i \approx 635$keV rather than 661.6keV (of ^{137}Cs). This deviation is unavoidable due to the coincidence technique for data acquisition. At low angles, the kinetic energy of the recoil electron becomes arbitrarily small, causing the target PMT to produce proportionally weak detection signals. Because we have employed a fixed discriminator set-point for coincidence logic generation, the target PMT will generally fail to produce a valid coincidence logic at low angles.

Therefore we report the results of the fit for only the (four) high-angle data. We obtain $E_i = (657.7 \pm 18.7)$keV and $E_a = (514.3 \pm 8.5)$keV, which contain the expected values of 661.6keV and 511keV respectively. We ascribe the large $\chi^2 = 6.4$ to the low degree of freedom ($\nu = 2$) used in the fitting. Overall, however, we observe variation in the final photon energy as suggested by the Compton shift formula.

4.3. Angular dependence of the cross-section

In our previous discussions we have already aluded to the Klein-Nishina cross-section as the true scattering model. In Figure 4 we show the experimentally measured scattering rates, and compare the Klein-Nishina and classical models. The results clearly favor the former. In particular, the symmetry suggested by the classical theory is not experimentally corroborated.
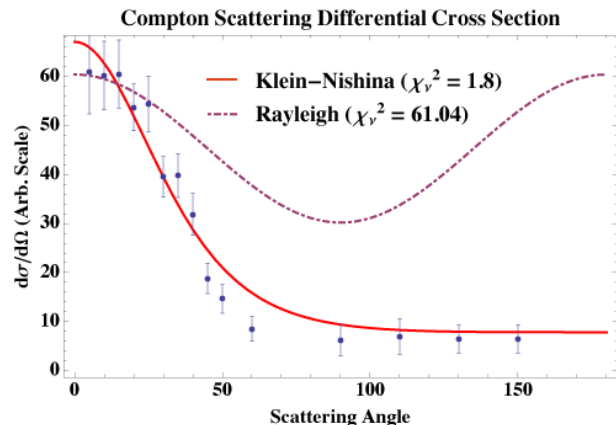

FIG. 4: The angular dependence of the scattering rate. Fits against the Klein-Nishina and classical cross-sections are performed, showing a definite preference for Klein-Nishina.

The scattering count and the associated error were obtained as follows. Recognizing that Compton scattering also occurs in the scatter PMT (note the Compton continuum in Fig. 2) we proceeded by summing all counts in the scatter spectrum. In addition to the statistical $\sqrt{N}$-error, we also made an estimate for the number of miscounts. This was done by counting the number of hits in the target spectrum that obviously did not correspond to Compton scattering; for instance, we observed a photopeak in the target spectrum due to the 661.6keV incident beam. We have also corrected the counts for detector inefficiency, i.e. by the probability for photons to traverse the PMT without interactions. We were able to combine Compton A and B data by normalizing both data sets by the intensity of the source.

We remark that the variation of the data about the fitted Klein-Nishina curve can be qualitatively explained by geometric effects. The "flattening" of the low-angle rate is a typical signature of a broad response function. Furthermore, the measured rate reaches the large-angle

baseline earlier than the theoretical curve. This is consistent since the interval of actual scattering angles about θ will reach the high-angle regime prior to θ.

4.4. Total cross-section

For the 611.6keV photons used in this experiment, the Klein-Nishina formula can be integrated over all solid angles to yield the total cross-section $\sigma_{KN} = 2.50 \times 10^{-25}\text{cm}^2$. The corresponding classical cross-section is $\sigma_{classical} = 6.59 \times 10^{-25}\text{cm}^2$. We have performed a direct measurement of the total cross-section by observing the rate of attenuation of the incident beam as it traverses through various plastics. Considering scattering to be a random process, we expect the the intensity to decrease exponentially ($\propto \exp(-\mu x)$) with increasing path length x at a rate $\mu = \rho n_e \sigma_{KN}$ where ρ is the density of the material and n_e is the electron density (per gram).

TABLE I: The total scattering cross-section σ_{KN} was calculated for the different target media

Target Medium	μ (cm)	ρ (g/cm^3)	σ_{KN} (10^{-25}cm^2)
Polycarbonate	0.092 ± 0.001	1.20 ± 0.05	2.43 ± 0.11
Polypropylene	0.074 ± 0.001	0.90 ± 0.05	2.40 ± 0.14
Polyvinyltoluene	0.0793 ± 0.0008	1.03 ± 0.05	2.36 ± 0.12

As shown in Table I, the measured total cross-sections are consistent with the Klein-Nishina theory.

5. ERROR ANALYSIS

The dominant complication in the experiment involves the finite geometry. For a fixed scatter PMT angle θ, we have performed a rudimentary assessment of the accessible scattering angles. By considering the endpoints of the equipment, we estimate (for Compton A) that the angular response function spans an extremely large interval of approximately $50°$ in forward scattering. The angular width decreases monotonically with increasing

θ, reaching approx. $20°$ by $\theta = 160°$. Hence, we conclude that the geometry is not a neglible factor. We have seen signatures of this effect in both Compton shift and scattering rate data. However, the large-angle measurements are more robust due to two factors: (1) the angular window decreases with increasing θ; and (2) the Klein-Nishina cross-section is uniform for large angles, so that the necessary convolution will have negligible impact on the result.

We have also remarked that the coincidence techniques will interfere with low-angle measurements. In the Compton A apparatus, we have adjusted the setup so that 661.6keV photon produces a roughly 7V pulse. The discriminator set-point was 2V. Hence, we expect the coincidence logic to be impaired near 189keV. According to Eq. 2, this corresponds to the kinetic energy of the recoil electron at a scattering angle of $\theta \approx 22°$. Therefore we expect underestimation of the scattering rate below $20°$ due to the coincidence logic. This is observed in Fig. 4.

Finally, we note that the sum of the energies of the scattered photopeak, and the recoil electron peak consistently add up to approx. 640keV, rather than the expected 661.6keV of the incident photon. We have not understood the cause of this phenomenon.

6. CONCLUSIONS

We have performed Compton scattering of 661.6keV photons. We have observed the Compton wavelength shift, illustrating the inadequacy of the classical model of light scattering. Small-angle measurements were complicated by the finite geometry and the data acquisition technique. However, a fit oo the large-angle data to the Compton shift formula produced an accurate estimate of the electron rest mass $E_a = (514.3 \pm 8.5)\text{keV/c}^2$ as well as the incident photon energy. We have also considered the scattering cross-section, in which the Klein-Nishina model prevails over the classical dipole radiation picture at $\chi_\nu^2 = 1.8$ vs. $\chi_\nu^2 = 61.0$. We believe that the chi_ν^2 statistic for the Klein-Nishina fit can be improved by addressing the geometric complications we have discussed.

[1] A. Melissinos, *Experiments in Modern Physics* (Academic Press, 1966).
[2] J. lab staff, *Compton scattering lab guide* (2007).